in the vehicle group (Fig. 7F). The inhibition of PAI-1 therefore enhances not only the rapid hematopoietic recovery in the early phase, but also the long-term self-renewal capacity of HSCs.

To compare the repopulating activity of long-term HSCs, a small number of primary Ly5.1$^+$ donor-derived hematopoietic cells after limiting dilution was transplanted into Ly5.2$^+$ mice (6×10^4 or 2×10^4 cells per mouse). Recipient Ly5.2$^+$ mice were thought to be successfully engrafted if Ly5.1$^+$ cells with the potential for multilineage differentiation were detected in excess of 1% of the total BM cells in the recipient (representative FACS profiles are shown in Supporting Information Fig. S8). The results demonstrated that the chimerism of Ly5.1$^+$ cells was higher in the PAI-1 inhibitor-treated group (1.26% ± 0.1% with 2×10^4 cells and 3.45% ± 1.09% with 6×10^4 cells) than in the vehicle-treated group (0.38% ± 0.26% with 2×10^4 cells and 1.04% ± 0.19% with 6×10^4 cells) (Fig. 7G). In addition, successful engraftment was achieved more often in the PAI-1 inhibitor-treated group (five of the five mice with 2×10^4 and 6×10^4 cells) than in the vehicle-treated group (one of the five mice with 2×10^4 cells and two of the five mice with 6×10^4 cells). Collectively, our results of the phenotypic (i.e., cell surface analysis) and repopulating (i.e., transplantation) assays revealed that inhibiting the PAI-1 activity during the early phase of reconstitution efficiently expands the long-term repopulating HSCs.

Discussion

This study was undertaken to elucidate the role of PAI-1, a negative regulator of the fibrinolytic pathway, in hematopoietic regeneration after irradiation-induced myeloablation. The results demonstrated the following: first, the expression levels of fibrinolytic factors, such as tPA and plasmin, are markedly augmented in endothelial and nonhematopoietic stromal cells, respectively, in the BM of mice after sublethal irradiation. Second, the PAI-1 expression is simultaneously upregulated in nonhematopoietic stromal cells, especially osteoblasts. Third, PAI-1 negatively regulates hematopoietic regeneration: the genetic deletion of PAI-1, as well as the administration of a PAI-1 inhibitor, activates the tPA-mediated fibrinolytic pathway, eventually accelerating hematopoietic regeneration. Finally, the inhibition of PAI-1 activity at an early phase of transplantation facilitates the recovery and maintenance of hematopoiesis (Supporting Information Fig. S9).

Previous studies have shown that the levels of fibrinolytic factors and their inhibitors are elevated in several tissues

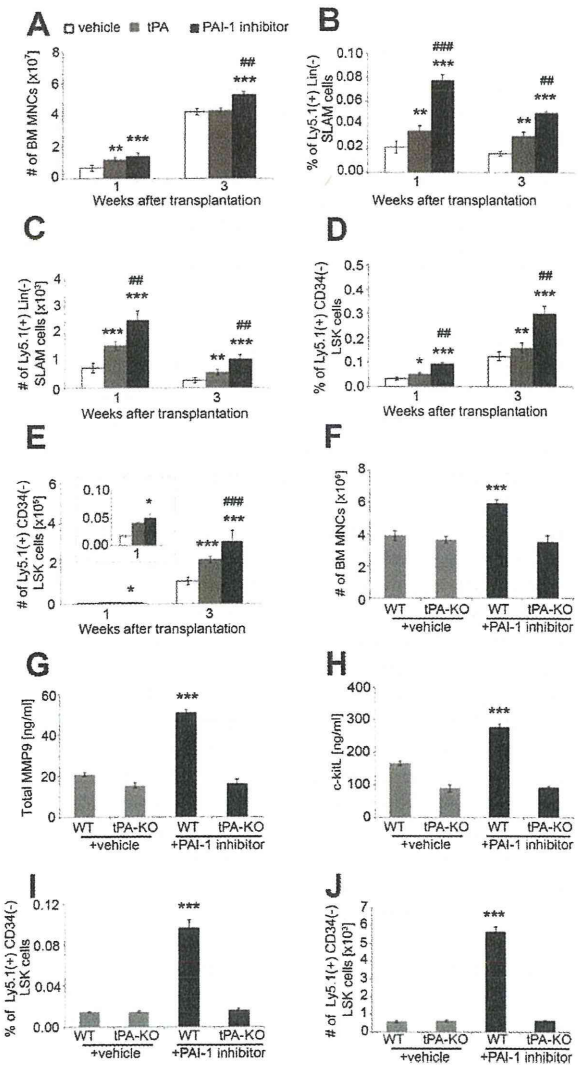

Figure 5. The PAI-1 inhibitor increases the proportion of hematopoietic stem cells (HSCs) during hematopoietic reconstitution. BM MNCs from the Ly5.1$^+$ donor mice (2.5×10^6) were transplanted into the 9 Gy-irradiated Ly5.2$^+$ mice, followed by repeated administration of saline (vehicle), tPA (10 mg/kg, i.p.), or the PAI-1 inhibitor (100 mg/kg, p.o.) for 5 consecutive days. **(A–E):** The results of the fluorescence-activated cell sorting (FACS) analysis of the HSCs in recipient mice. BM MNCs were obtained at the indicated time points from four long leg bones per mouse, and were pooled and subjected to a FACS analysis. (A): The total number of BM MNCs per recipient. (B): The proportion of Lin$^-$ SLAM cells among the donor-derived Ly5.1$^+$ cells, (C) the total number of Lin$^-$SLAM cells, (D) the proportion of CD34$^-$LSK cells among the donor-derived Ly5.1$^+$ cells, and (E) the total number of CD34$^-$LSK cells were calculated at 1 and 3 weeks. The bars in white, gray, and black represent the vehicle-, tPA-, and PAI-1 inhibitor-treated mice, respectively. The data from four independent experiments are expressed as the means ± SD ($n = 12$ for each condition). The inset graph in (E) is a magnification of the data at 1 week. *, $p < .05$; **, $p < .01$; ***, $p < .001$ versus the vehicle group, ##, $p < .01$; ###, $p < .001$ versus the tPA group. **(F–J):** In separate experiments, WT (Ly5.2$^+$, tPA$^{+/+}$) or tPA-KO (Ly5.2$^+$, tPA$^{-/-}$) mice were exposed to 9 Gy radiation and transplanted with 2.5×10^6 BM MNCs (Ly5.1$^+$, tPA$^{+/+}$). Either vehicle or a PAI-1 inhibitor was administered to the recipient mice daily for 5 consecutive days beginning the day after the BM infusion. Plasma and BM MNCs were collected 1 week after transplantation. (F): The total number of isolated BM MNCs per mouse at the indicated time points. The plasma levels of total MMP-9 (G) and c-kitL (H) in the recipient mice. Donor-derived Ly5.1$^+$ cells were gated, and the proportion of CD34$^-$LSK cells (I) and the total number of CD34$^-$LSK cells (J) in the recipient BM were analyzed. The data from three independent experiments are shown as the means ± SD ($n = 6$ for each condition). ***, $p < .001$ by one-way ANOVA. Abbreviations: BM, bone marrow; MNC, mononucleic cell; PAI-1, plasminogen activator inhibitor-1; tPA, tissue-type plasminogen activator; WT, wild type; MMP9, matrix metalloproteinase 9.

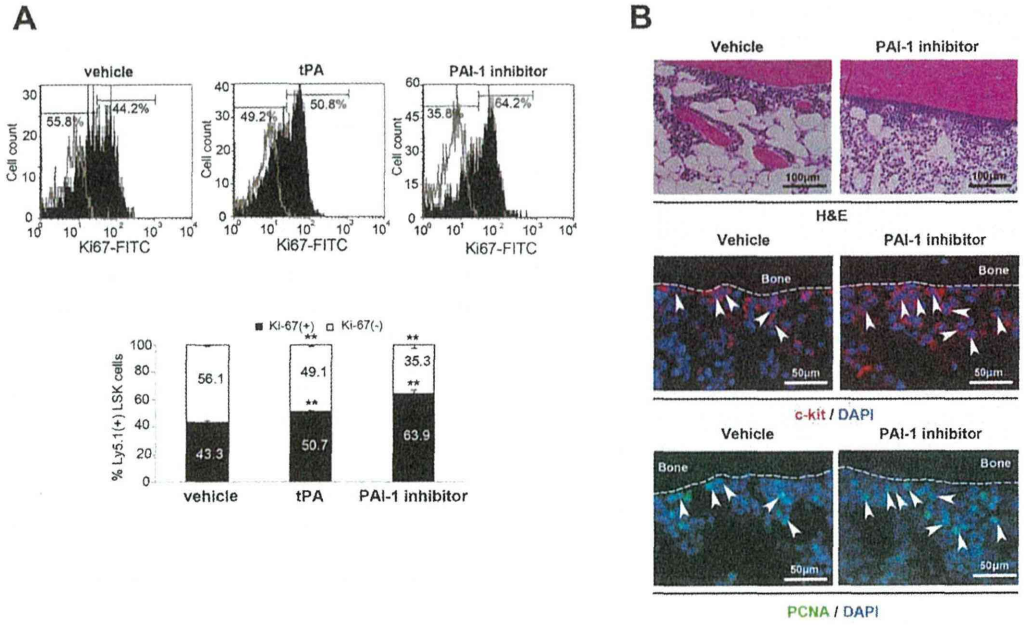

Figure 6. The PAI-1 inhibitor promotes hematopoietic stem cell (HSC) proliferation. Ly5.2$^+$ mice were exposed to 9 Gy radiation and transplanted with 2.5 $\times$ 10^6 Ly5.1$^+$ BM MNCs. Thereafter, vehicle or the PAI-1 inhibitor was administered daily to the mice for 5 consecutive days, and the mice were sacrificed on day 7 for the fluorescence-activated cell sorting (FACS) and BM histological analyses. **(A):** Representative FACS profiles of the Ki67-expression in the donor-derived Ly5.1$^+$ LSK cells. BM MNCs were collected, and the proportion of *Ki67$^+$ cells among the Ly5.1$^+$ donor-derived HSCs was analyzed. Isotype-matched control IgG was used to identify the Ki67$^-$ cells.* The proportion of Ki67$^+$ or Ki67$^-$ cells is shown above each histogram. The average proportion of Ki67$^+$ Ly5.1$^+$ LSK cells from three independent experiments (each with two mice) is shown in the right panel. **, $p < .01$ versus the vehicle group by one-way ANOVA followed by Bonferroni post-test. **(B):** Representative H&E staining (left panel set) or fluorescent immunostaining (c-kit [red] in the middle panel set; PCNA [green] in the right panel set) of serial sections of bone. Nuclei were counterstained with DAPI (blue). Arrowheads indicate positive cells. Abbreviations: FITC, fluorescein isothiocyanate; DAPI, 4′,6-diamidino-2-phenylindole; PAI-1, plasminogen activator inhibitor-1; H&E, hematoxylin and eosin; PCNA, proliferation cell nuclear antigen; tPA, tissue-type plasminogen activator.

following irradiation [22–24]. However, the dynamics of fibrinolytic system factors, particularly PAI-1, in hematopoietic regeneration of the BM have not been elucidated. This study revealed, for the first time, that irradiation has a substantial impact on the fibrinolytic system in the BM. Upon irradiation, the levels of fibrinolytic factors and PAI-1 in the BM fluid increased dramatically (~30-fold), in sharp contrast to the moderate increase in these factors in the plasma (1.8–3-fold). Of note, their levels in the BM fluid were 1 or 2 orders of magnitude higher than those in the plasma (e.g., 300 and 8 ng/ml of PAI-1 in the BM fluid and plasma, respectively), demonstrating that BM cells have a potent capacity to produce fibrinolytic factors and PAI-1 upon irradiation. In good agreement with these in vivo results, *the results of the in vitro cultured cell experiments demonstrated* that nonhematopoietic BM stromal cells readily produce tPA, plasmin, and PAI-1 after irradiation.

On closer inspection by immunohistochemistry, we identified nonhematopoietic cells, especially stromal cells, as the primary source of fibrinolytic factors and PAI-1. Our data in the irradiated PAI-1 KO mice (recipient), which have undetectable levels of PAI-1 in the plasma after transplantation of normal hematopoietic cells (PAI-1$^{+/+}$), suggested that the marked increase in PAI-1 after irradiation does not originate from donor hematopoietic cells. Nonhematopoietic stromal cells in the BM thus play a significant role in repairing the myeloablated hematopoietic microenvironment. This is not surprising, because the irradiation of mice with a lethal dose of radiation eradicates the hematopoietic cells and their progenitor cells, but not nonhematopoietic cells [25, 26].

We also elucidated the mechanism by which PAI-1 regulates the hematopoietic regeneration in the BM. A previous study by Hattori and colleagues demonstrated that activation of the fibrinolytic pathway by administration of recombinant tPA results in the conversion of the transmembrane form to the soluble form of c-kitL [6], a hematopoiesis-promoting factor. They suggested that activated plasmin subsequently transforms MMP-2/9 into active forms, which in turn release c-kitL from stromal cells. It is therefore likely that PAI-1 activity prevents the hematopoietic regeneration in the BM by inhibiting the fibrinolytic pathway and c-kitL release. Our results showing that the suppression of PAI-1 activity either by a pharmacological approach or by the genetic deletion of the PAI-1 gene can elevate the tPA/plasmin activity, promote c-kitL production, and lead to the rapid recovery of hematopoiesis after myeloablation. Although other products of fibrinolytic degradation may also promote engraftment, these results support the critical role of c-kitL production in the improvement of engraftment by PAI-1 inhibition.

Emerging evidence suggests that PAI-1 expression generally limits tissue repair by negatively regulating the fibrinolytic environment and by inhibiting cell migration [27]. For example, the skin wound healing process is accelerated in PAI-1-deficient mice [28]. PAI-1 KO mice are also protected against liver fibrosis [29] and radiation enteropathy [24]. In terms of tissue

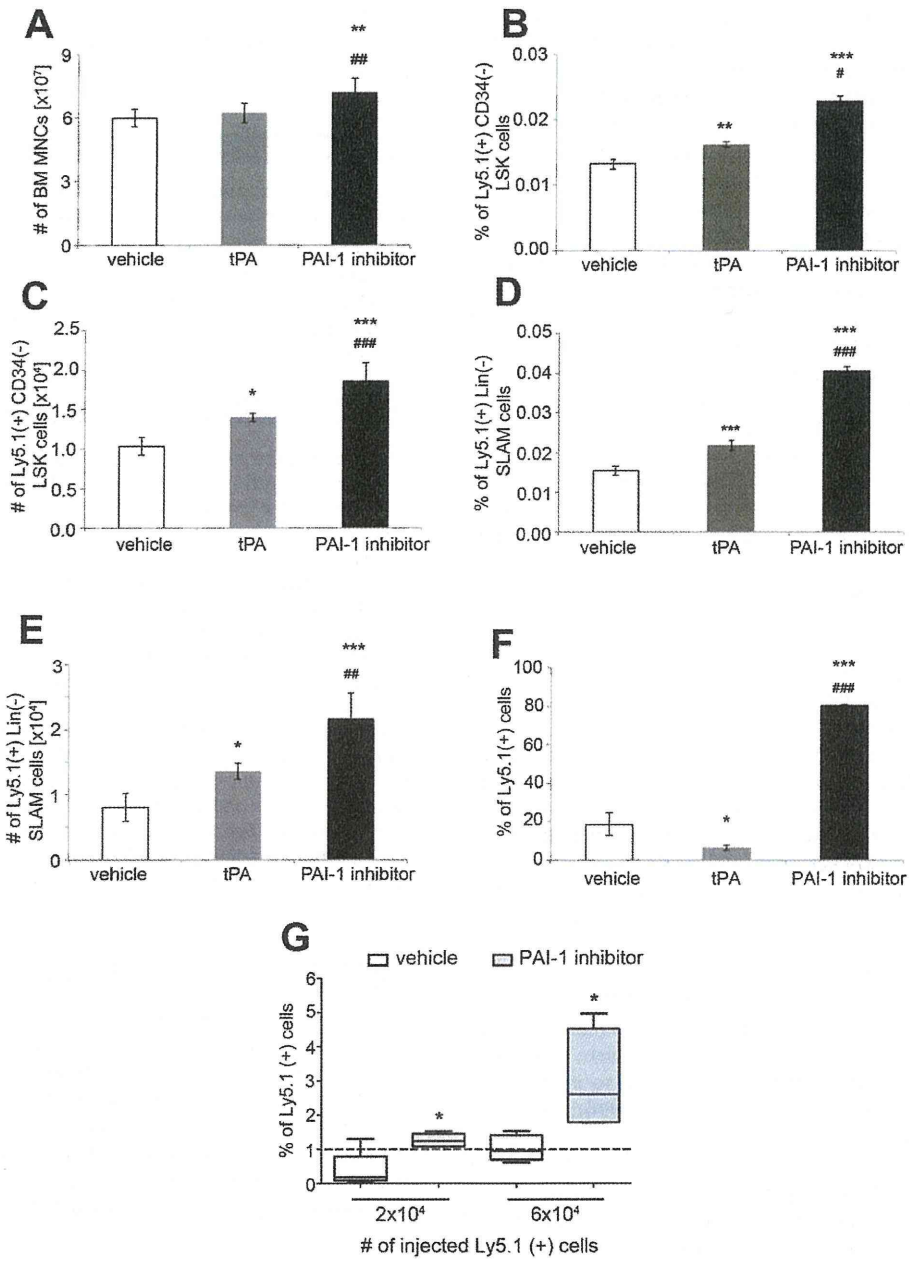

Figure 7. The PAI-1 inhibitor enhances the self-renewal capacity of hematopoietic stem cells. **(A–E):** The Ly5.2$^+$ mice were exposed to 9 Gy radiation, followed by transplantation with 2.5 × 10^6 Ly5.1$^+$ BM MNCs. They were administered the vehicle, tPA, or the PAI-1 inhibitor daily for 5 consecutive days. BM MNCs were collected 15 weeks after transplantation. BM MNCs were obtained from four long leg bones per mouse, and were pooled for the analysis of (A) the total number of donor-derived Ly5.1$^+$ BM MNCs, (B) the proportion of CD34$^-$LSK cells among Ly5.1$^+$ cells, (C) the total number of CD34$^-$LSK cells, (D) the proportion of Lin$^-$SLAM cells among Ly5.1$^+$ cells, (E) the total number of Lin$^-$SLAM cells. The data from four independent experiments are shown ($n = 12$ for each condition). *, $p < .05$; **, $p < .01$; ***, $p < .001$ versus the vehicle group; $^{\#}$, $p < .05$; $^{\#\#}$, $p < .01$; $^{\#\#\#}$, $p < .001$ versus the tPA group. The p value was calculated by one-way ANOVA followed by Bonferroni post-test. **(F):** The chimerism of donor-derived Ly5.1$^+$ cells in the secondary recipients. Donor-derived Ly5.1$^+$ BM MNCs (1 × 10^6) in the primary recipient mice were retransplanted, together with 5 × 10^5 Ly5.2$^+$ competitor cells, into the 9 Gy-irradiated Ly5.2$^+$ secondary recipient mice. BM cells were analyzed 12 weeks after the secondary transplantation. The data from three independent experiments are shown ($n = 10$ for each condition). *, $p < .05$; ***, $p < .001$ versus the vehicle group; $^{\#\#\#}$, $p < .001$ versus the tPA group. **(G):** The chimerism of a small number of donor-derived Ly5.1$^+$ cells in the secondary recipients. A total of 2 × 10^4 or 6 × 10^4 Ly5.1$^+$ BM cells from the primary recipient mice, with 5 × 10^5 Ly5.2$^+$ competitor cells, were transplanted into the 9 Gy-irradiated Ly5.2$^+$ secondary recipient mice. Twelve weeks after the secondary transplantation, the chimerism of donor cells in the BM was evaluated. The boxes in white and gray represent the chimerism of donor-derived Ly5.1$^+$ cells in the vehicle- and PAI-1 inhibitor-treated mice, respectively. The horizontal lines in the box represent the median chimerism, and bars indicate the SD. The dashed line indicates the cut-off value (1%). Data from two independent experiments are shown ($n = 5$ for each condition). *, $p < .05$ versus the vehicle group. Abbreviations: BM, bone marrow; MNC, mononucleic cell; PAI-1, plasminogen activator inhibitor-1; tPA, tissue-type plasminogen activator.

regeneration, Galipeau and colleagues have demonstrated that mesenchymal stem cells (MSCs) derived from PAI-1 KO mice exhibited higher regenerative potential than those from WT mice [30]. Furthermore, chemical manipulation of the PAI-1 activity improves the engraftment of MSCs, defining PAI-1 as a negative regulator of transplanted stem cell survival in vivo [30]. This study clarified the active involvement of PAI-1 in the hematopoietic regeneration after irradiation.

Proper treatment of the initial stage of hematopoietic recovery and the prevention of premature HSC exhaustion could therefore significantly improve the clinical outcome of transplantation [1, 2]. In this regard, our study demonstrated that, despite a short period of administration, the suppression of the PAI-1 activity by a low molecular weight compound could induce both rapid hematopoietic regeneration through increased cycling of HSCs and expansion of the long-term HSCs. This opens a new avenue for improving HSCT. It should be emphasized that the PAI-1 inhibitor does not induce HSC exhaustion or malignancy in spite of its potent ability to increase the cycling of HSCs. The results of this study clearly demonstrated that c-kit$^+$ HSPCs in the group treated with the PAI-1 inhibitor preferentially localized to the BM niche, just like in the vehicle-treated group, suggesting that the interaction between the hematopoietic progenitor cells and niche is maintained even after the treatment with a PAI-1 inhibitor. This may be a plausible explanation for why the PAI-1 inhibitor does not induce HSC exhaustion.

Both the PAI-1 inhibitor and tPA theoretically activate the fibrinolytic pathway and the subsequent hematopoietic regeneration, but their effects in vivo in animals appear to be different. This is partly explained by the differences in the routes of administration between tPA and the PAI-1 inhibitor, as well as the doses, mechanisms of action, and/or half-lives of these agents. Recombinant tPA is administered intravenously (a large amount of tPA is given directly into the circulation), and immediately activates the fibrinolytic pathway, but its half-life is only a few minutes [17]. In contrast, the PAI-1 inhibitor was given orally, and was absorbed in the gut, entered into the circulation gradually, inhibited the PAI-1 moiety, and subsequently upregulated the tPA activity leading to its effects on the fibrinolytic pathway. The half-life of the PAI-1 inhibitor is much longer (6.5 hour) than that of tPA.

It is also important to note that tPA administration itself increased the PAI-1 level, suggesting a potential negative feedback effect in this pathway and limits to the therapeutic benefits of tPA for hematopoietic regeneration. In addition, the repopulating capacity of HSCs in tPA-treated mice showed a slight decrease, suggesting that tPA treatment may induce HSC exhaustion. It should also be mentioned that PAI-1 regulates not only tPA, but also other proteins (i.e., vitronectin, urokinase-type plasminogen activator (uPA), and low density lipoprotein receptor (LDLR)) [5, 31, 32] and thereby has an impact on broader biological systems.

Conclusion

In conclusion, our study provides the first direct evidence that PAI-1 is a negative regulator of hematopoietic regeneration, and that the inhibition of PAI-1 activity, either genetically or by a low molecular weight compound, significantly improves donor-derived hematopoiesis after transplantation. Our findings give new insights into the treatment of HSCT and for clinical transplantation medicine.

Acknowledgments

We appreciate the help of Dr. Koichi Hattori (Institute of Medical Science, University of Tokyo, Japan) for kindly providing the tPA KO mice. We thank Dr. Nobuo Watanabe (Tokai University School of Medicine, Japan) for helpful discussion and wrote the manuscript. We also thank the members of the Research Center for Regenerative Medicine of Tokai University, especially Tomomi Takanashi, Kozue Hiyama, and Tomoko Uno, for the technical support. We thank the members of the Animal Care Center of Tokai University for their meticulous care of the experimental animals. This work was supported by Japanese Grants-in-Aid for Scientific Research from the Ministry of Education, Culture, Sports, Science and Technology (MEXT), from the Ministry of Health, Labor and Welfare (MHLW), from the National Institute of Biomedical Innovation (NIBIO), from the Japan Science and Technology Agency (JST), and from the Tokai University School of Medicine Research Aid. Special thanks are due to the MARA Education Foundation, Malaysia, for supporting the scholarship awarded to A.A.I.

Author Contributions

A.A.I.: collection and assembly of data, data analysis and interpretation, and manuscript writing; T.Y.: conception and design, data analysis and interpretation, manuscript writing, and financial support; M.O.: data analysis and interpretation; T.D.: provision of study material; C.v.Y.d.S.: manuscript writing; T.M.: provision of study material, data analysis and interpretation, and manuscript writing; K.A.: conception and design, data analysis and interpretation, financial support, and final approval of manuscript.

Disclosure of Potential Conflicts of Interest

The authors indicate no potential conflicts of interest.

References

1 Perumbeti A, Sacher RA. Hematopoietic Stem Cell Transplantation. Available at http://emedicine.medscape.com/article/208954. Accessed November 30, 2012.

2 Chawla R, Davies HD. Infections After Bone Marrow Transplantation. Available at http://emedicine.medscape.com/article/1013470. Accessed September 13, 2012.

3 Kolev K, Machovich R. Molecular and cellular modulation of fibrinolysis. Thromb Haemost 2003;89:610–621.

4 Collen D, Lijnen HR. Basic and clinical aspects of fibrinolysis and thrombolysis. Blood 1991;78:3114–3124.

5 Diebold I, Kraicun D, Bonello S et al. The 'PAI-1 paradox' in vascular remodeling. Thromb Haemost 2008;100:984–991.

6 Heissig B, Lund LR, Akiyama H et al. The plasminogen fibrinolytic pathway is required for hematopoietic regeneration. Cell Stem Cell 2007;1:658–670.

7 Heissig B, Ohki M, Ishihara M et al. Contribution of the fibrinolytic pathway to hematopoietic regeneration. J Cell Physiol 2009;221:521–525.

8 Izuhara Y, Takahashi S, Nangaku M et al. Inhibition of plasminogen activator inhibitor-1: Its mechanism and effectiveness on coagulation and fibrosis. Atertio Thromb Vasc Biol 2008;28:672–677.

9 Yamaoka N, Kodama H, Izuhara Y et al. Structure-activity relationships of new N-acylanthranilic acid derivatives as plasminogen activator inhibitor-1 inhibitors. Chem Pharm Bull (Tokyo) 2011;59:215–224.
10 Izuhara Y, Yamaoka N, Kodama H et al. A novel inhibitor of plasminogen activator inhibitor-1 provides antithrombotic benefits devoid of bleeding effect in nonhuman primates. J Cereb Blood Flow Metab 2010;30: 904–912.
11 Carmeliet P, Kieckens L, Schoonjans L et al. Plasminogen activator inhibitor-1 gene-deficient mice. I. Generation by homologous recombination and characterization. J Clin Invest 1993;92:2746–2755.
12 Carmeliet P, Stassen JM, Schoonjans L et al. Plasminogen activator inhibitor-1 gene-deficient mice. II. Effects on hemostasis, thrombosis, and thrombolysis. J Clin Invest 1993;92:2756–2760.
13 Carmeliet P, Schoonjans L, Kieckens L et al. Physiological consequences of loss of plasminogen activator gene function in mice. Nature 1994;368:419–424.
14 Nilsson SK, Johnston HM, Coverdale JA. Spatial localization of transplanted hemopoietic stem cells: Inferences for the localization of stem cell niches. Blood 2001;97:2293–2299.
15 Yahata T, Muguruma Y, Yumino S et al. Quiescent human hematopoietic stem cells in the bone marrow niches organize the hierarchical structure of hematopoiesis. Stem Cells 2008;26:3228–3236.
16 Zhang B, Ho YW, Huang Q et al. Altered microenvironmental regulation of leukemic and normal stem cells in chronic myelogenous leukemia. Cancer Cell 2012;21:577–592.
17 Narita M, Bu G, Herz J et al. Two receptor systems are involved in the plasma clearance of tissue-type plasminogen activator (t-PA) in vivo. J Clin Invest 1995;96:1164–1168.
18 Na Nakorn T, Traver D, Weissman IL et al. Myeloerythroid-restricted progenitors are sufficient to confer radioprotection and provide the majority of day 8 CFU-S. J Clin Invest 2002;109:1579–1585.
19 Jaroscak J, Goltry K, Smith A et al. Augmentation of umbilical cord blood (UCB) transplantation with ex vivo-expanded UCB cells: Results of a phase 1 trial using the AastromReplicell System. Blood 2003;101:5061–5067.
20 Ando K, Yahata T, Sato T et al. Direct evidence for ex vivo expansion of human hematopoietic stem cells. Blood 2006;107:3371–3377.
21 Dahlberg A, Delaney C, Bernstein ID. Ex vivo expansion of human hematopoietic stem and progenitor cells. Blood 2011;117: 6083–6090.
22 Rao JS, Rayford A, Yamamoto M et al. Modulation of fibrinolysis by ionizing radiation. J Neurooncol 1994;22:161–171.
23 Zhao W, O'Malley Y, Robbins ME. Irradiation of rat mesangial cells alters the expression of gene products associated with the development of renal fibrosis. Radiat Res 1999;152:160–169.
24 Milliat F, Sabourin JC, Tarlet G et al. Essential role of plasminogen activator inhibitor type-1 in radiation enteropathy. Am J Pathol 2008;172:691–701.
25 Rubin P. Law and order of radiation sensitivity. Absolute versus relative. Front Radiat Ther Oncol 1989;23:7–40.
26 Sugrue T, Lowndes NF, Ceredig R. Mesenchymal stromal cells: Radio-resistant members of the bone marrow. Immunol Cell Biol 2013;91:5–11.
27 Czekay RP, Wilkins-Port CE, Higgins SP et al. PAI-1: An Integrator of Cell Signaling and Migration. Int J Cell Biol 2011;2011: 562481.
28 Chan JC, Duszczyszyn DA, Castellino FJ et al. Accelerated skin wound healing in plasminogen activator inhibitor-1-deficient mice. Am J Pathol 2001;159:1681–1688.
29 Bergheim I, Guo L, Davis MA et al. Critical role of plasminogen activator inhibitor-1 in cholestatic liver injury and fibrosis. J Pharmacol Exp Ther 2006;316:592–600.
30 Copland IB, Lord-Dufour S, Cuerquis J et al. Improved autograft survival of mesenchymal stromal cells by plasminogen activator inhibitor 1 inhibition. Stem Cells 2009;27: 467–477.
31 Balsara RD, Ploplis VA. Plasminogen activator inhibitor-1: The double-edged sword in apoptosis. Thromb Haemost 2008;100:1029–1036.
32 Herz J, Strickland DK. LRP: A multifunctional scavenger and signaling receptor. J Clin Invest 2001;108:779–784.


See www.StemCells.com for supporting information available online.

Am J Physiol Renal Physiol 308: F614–F626, 2015.
First published January 13, 2015; doi:10.1152/ajprenal.00616.2014.

Podocyte injury-driven intracapillary plasminogen activator inhibitor type 1 accelerates podocyte loss via uPAR-mediated β_1-integrin endocytosis

Namiko Kobayashi,[1] Toshiharu Ueno,[1] Kumi Ohashi,[1] Hanako Yamashita,[1] Yukina Takahashi,[1] Kazuo Sakamoto,[1] Shun Manabe,[1] Satoshi Hara,[1] Yasutoshi Takashima,[1] Takashi Dan,[2] Ira Pastan,[3] Toshio Miyata,[2] Hidetake Kurihara,[4] Taiji Matsusaka,[5] Jochen Reiser,[6] and Michio Nagata[1]

[1]*Department of Pathology, Graduate School of Comprehensive Human Sciences, University of Tsukuba, Ibaraki, Japan;* [2]*Center for Translational and Advanced Research, Tohoku University Graduate School of Medicine, Sendai, Miyagi, Japan;* [3]*Laboratory of Molecular Biology, Center for Cancer Research, National Cancer Institute, National Institutes of Health, Bethesda, Maryland;* [4]*Department of Anatomy, Juntendo University School of Medicine, Bunkyo, Tokyo, Japan;* [5]*Department of Internal Medicine, Institute of Medical Science, Tokai University School of Medicine, Isehara, Kanagawa, Japan; and* [6]*Department of Medicine, Rush University, Chicago, Illinois*

Submitted 11 November 2014; accepted in final form 8 January 2015

Kobayashi N, Ueno T, Ohashi K, Yamashita H, Takahashi Y, Sakamoto K, Manabe S, Hara S, Takashima Y, Dan T, Pastan I, Miyata T, Kurihara H, Matsusaka T, Reiser J, Nagata M. Podocyte injury-driven intracapillary plasminogen activator inhibitor type 1 accelerates podocyte loss via uPAR-mediated β_1-integrin endocytosis. *Am J Physiol Renal Physiol* 308: F614–F626, 2015. First published January 13, 2015; doi:10.1152/ajprenal.00616.2014.— Podocyte-endothelial cell cross-talk is paramount for maintaining the filtration barrier. The present study investigated the endothelial response to podocyte injury and its subsequent role in glomerulosclerosis using the podocyte-specific injury model of NEP25/LMB2 mice. NEP25/LMB2 mice showed proteinuria and local podocyte loss accompanied by thrombotic microangiopathy on *day 8*. Mice showed an increase of glomerular plasminogen activator inhibitor type 1 (PAI-1) mRNA and aberrant endothelial PAI-1 protein already on *day 1*, before thrombosis and proteinuria. A PAI-1-specific inhibitor reduced proteinuria and thrombosis and preserved podocyte numbers in NEP25/LMB2 mice by stabilization of β_1-integrin translocation. Heparin loading significantly reduced thrombotic formation, whereas proteinuria and podocyte numbers were unchanged. Immortalized podocytes treated with PAI-1 and the urokinase plasminogen activator (uPA) complex caused significant cell detachment, whereas podocytes treated with PAI-1 or uPA alone or with the PAI-1/uPA complex pretreated with an anti-uPA receptor (uPAR) antibody failed to cause detachment. Confocal microscopy and cell surface biotinylation experiments showed that internalized β_1-integrin was found together with uPAR in endocytotic vesicles. The administration of PAI-1 inhibitor or uPAR-blocking antibody protected cultured podocytes from cell detachment. In conclusion, PAI-1/uPA complex-mediated uPAR-dependent podocyte β_1-integrin endocytosis represents a novel mechanism of glomerular injury leading to progressive podocytopenia. This aberrant cross-talk between podocytes and endothelial cells represents a feedforward injury response driving podocyte loss and progressive glomerulosclerosis.

podocyte; plasminogen activator inhibitor type 1; endocytosis; integrin; kidney; pathology

PODOCYTE INJURY and the subsequent cell loss promote glomerulosclerosis in various glomerular diseases (7, 8, 21, 43). However, there is limited information describing the detailed mechanism of podocyte injury-induced glomerulosclerosis. In the remnant kidney model, segmental podocyte loss was accompanied by synechiae formation to Bowman's capsule, leading to segmental sclerosis (27, 28). A more progressive podocyte loss model was followed by Notch1-mediated parietal epithelial cell migration leading to collapsing focal segmental glomerulosclerosis (FSGS); thus, podocyte loss triggers a maladaptive extracapillary response leading to sclerosis (39).

The glomerular filtration barrier is composed of podocytes, the glomerular basement membrane (GBM), and endothelial cells (8). Homeostatic regulation of filtration barrier function has been suggested to be maintained by cross-talk signaling between podocytes and endothelial cells. Electron microscopy showed a close association of endothelial cell abnormalities and overlying podocyte injury in various models of glomerulosclerosis, suggesting a causal relationship between these two cells (12, 22). Bevacizumab is an anti-VEGF antibody used in the treatment of cancer that occasionally causes glomerular thrombotic microangiopathy (TMA), and mice with podocyte-specific VEGF depletion have intracapillary lesions similar to TMA (12). These observations suggest that podocyte-derived VEGF preserves intracapillary homeostasis; however, the molecular basis of the intracapillary response to podocyte injury and its role in progressive glomerular damage has not been delineated. Blockade of endothelial VEGF transport in mice deficient in EH-domain containing 3/4 caused podocyte foot processes effacement (13). Shear stress in glomerular endothelial cells in vitro changed the actin arrangement in cocultured podocytes via ERK5-mediated vasodilator-stimulated phosphoprotein phosphorylation (36). Additionally, transient podocyturia and heavy proteinuria accompany pregnancy-induced hypertension, of which the pathophysiological base is severe endothelial cell injury (1). These findings suggest that podocyte injury triggers intracapillary-derived aberrant podocyte danger signals that underlie glomerular diseases.

Plasminogen activator inhibitor type 1 (PAI-1) is synthesized by several cell types and is known to inhibit fibrinolysis to stop bleeding by inactivating tissue plasminogen activator and urokinase plasminogen activator (uPA) (31, 44). Additionally, PAI-1 has several pleiotropic actions, including effects on cell survival, proliferation, motility, and mobility (9, 24). Notably, PAI-1 is not expressed in normal kidney glomeruli (10). Instead, PAI-1 is upregulated in glomeruli of patients with FSGS and membranous nephropathy, both of which are

Address for reprint requests and other correspondence: M. Nagata, Kidney and Vascular Pathology, Faculty of Medicine, Univ. of Tsukuba, 1-1-1, Ten-nodai, Tsukuba, Ibaraki 305-8577, Japan (e-mail: nagatam@md.tsukuba.ac.jp).

podocyte diseases (14, 29, 45). PAI-1 interacts with the uPA receptor (uPAR), which is upregulated in podocytes undergoing injury, and the soluble form of uPAR can drive the onset of FSGS via interactions with the podocyte integrin system (41, 42). These findings suggest a novel action of glomerular PAI-1 on podocyte diseases.

The present study aimed to investigate the glomerular intracapillary response to primary podocyte injury and its role in disease progression using a transgenic murine model of podocyte-selective injury (26). Our results showed that aberrant intracapillary signals associated with podocyte injury accelerated podocyte loss due to local PAI-1/uPA complex formation, which mediated its effect through uPAR-dependent β_1-integrin endocytosis by podocytes. This suggests a novel mechanism for a vicious cycle of podocyte loss. Additionally, since PAI-1 inhibition ameliorates this exacerbated podocyte loss, our work suggests a novel therapeutic option for podocyte injury-driven glomerulosclerosis.

MATERIALS AND METHODS

Animal Experiments

We used well-established NEP25 mice treated with an immunotoxin (LMB2 NEP25/LMB2 mice) (26), a FSGS model driven by podocyte-specific injury. NEP25 mice with the C57BL/6J genetic background selectively express human CD25 on podocytes. Podocyte-specific injury was induced by human CD25-specific antibody (LMB2), as previously described (26, 39). The toxin was given once; it disappeared after 35 min and set in motion a cascade leading to podocyte depletion. Mice were treated humanely and housed in animal facilities with free access to food and water, according to protocols approved by the Institutional Animal Use and Care Committee of the University of Tsukuba (Registered No. 11-305).

Protocols

Protocol 1: microangiopathic assessment of podocyte injury in NEP25 mice injected with LMB2. NEP25 mice aged 12–18 wk (n = 32) were randomly divided into two groups: *1*) NEP25/LMB2 mice anesthetized with isoflurane and injected with LMB2 intravenously (n = 26, 4 ng/g body wt) on *day 0* and *2*) NEP25/PBS mice injected with PBS intravenously as controls (n = 6). The LMB2 dosages used in this experiment induces severe nephrosis and mice died at 2 wk, as previously described (26, 39). Our preliminary study showed no proteinuria in wild-type littermate mice treated with LMB2. Histopathology was conducted in both groups (with LMB2: n = 6 and with PBS: n = 6). Renal samples were obtained by biopsy (on *days −1* and *8*) and autopsy at death (on *day 12*). Proteinuria was measured on *days −1*, *0*, *5*, *8*, and *12* after injection and estimated as the urinary protein-to-creatinine ratio. For real-time PCR, glomeruli were isolated from each animal, NEP/LMB2 mice on *days −1* (n = 5), *1* (n = 5), *8* (n = 5), and 12 (n = 5), and were statistically analyzed.

Protocol 2: effect of PAI-1 inhibition on NEP25 mice injected with LMB2. NEP25/LMB2 mice aged 12–18 wk (n = 24) were divided into two groups: *1*) PAI-1 inhibitor-treated NEP25/LMB2 mice (NEP25/LMB2 + PI) and *2*) vehicle-treated NEP25/LMB2 mice (NEP25/LMB2 + VH). NEP25/LMB2 + PI mice were administered the PAI-1 inhibitor TM5484 (10 μg/g body wt in 0.5% carboxymethyl cellulose sodium, n = 13) orally for 12 days. As the half-life of LMB2 is 35 min, the PAI-1 inhibitor was initially administered 2 h after LMB2 injection. NEP25/LMB2 + VH mice (n = 11) were administered vehicle orally for 12 days after LMB2 injection. The details of PAI-1 inhibitor are summarized below. Histology and real-time PCR were performed on biopsies from NEP25/LMB2 + PI (n = 8) and NEP25/LMB2+VH (n = 6) mice on *days −1* and *8* and on *day 12* at death. Biopsy samples contained over 30 glomeruli in a single section. After LMB2 injection, 24-h urine samples were collected on *days −1*, *0*, *5*, *8*, and *12*. Glomeruli were isolated from both groups (n = 5 mice/group) at death and used for real-time PCR.

The PAI-1 inhibitor TM5484 (molecular weight: 384.8 g/mol, clogP: 2.32) was designed based on structures of the PAI-1 inhibitor TM5007 (19). TM5007 was the initial compound identified virtually by structure-based drug design after undergoing a docking simulation that selected for compounds that fit within the cleft of PAI-1 (s3A in the human PAI-1 three-dimensional structure) and was accessible to insertion of the reactive center loop (18, 19). The design of TM5484 was processed by an extensive structural activity relationship study among >450 novel derivatives of TM5007 with comparatively low molecular weight (400–550 g/mol) without symmetrical structure (17). The inhibitory activity of TM5484 was shown in vitro by a chromogenic assay (IC_{50}: 3.56 μM), and its specificity was confirmed by demonstrating that it did not inhibit other serpins, such as antithrombin III and α_2-antiplasmin. A repeated dose toxicity study of TM5484 was assessed for 2 wk in five rats per gender per group, and no adverse effect level was concluded at 30 mg/kg. Regarding the reverse mutation Ames test, evaluation of TM5484 produced a negative result. The effect of TM5484 on human *ether-a-go-go*-related gene (hERG) electric current was investigated in human embryonic kidney-293 cells transfected with the hERG gene. TM5484 was found not to have an effect on hERG electric current at concentrations up to 10 μmol/l. We assessed the average bleeding time in NEP25/PBS mice by tail cut (n = 3). Average bleeding times after TM5484 treatment were 165 ± 39.7 s at preadministration, 375 ± 68.7 s at maximal time (2 h for TM5484, $P < 0.05$ vs. preadministration), and 341.7 ± 3.33 s at 24 h, which indicated the effects of TM5484 in the NEP25 mouse model.

Protocol 3: effect of heparin loading on NEP25/LMB2 mice. NEP25/LMB2 mice aged 12–18 wk (n = 10) were divided into two groups: *1*) NEP25/LMB2 mice treated with 25 units of heparin sodium (Fuji Pharma, Tokyo, Japan) through subcutaneous injection twice daily from *days −1* to *11* (NEP25/LMB2 + Hep; n = 5) and *2*) NEP25/LMB2 mice treated with PBS (NEP25/LMB2 + PBS; n = 5), which were considered controls. The anticoagulant effect of heparin was determined by the coagulation time, as revealed by a recalcification coagulation assay (16). The dosage of heparin sodium used was determined by keeping the coagulation time three times longer than that for control mice. Histology was performed on *day −1* by biopsy and on *day 12* at death. Proteinuria was estimated on *days 0*, *5*, *8*, and *12*. Number of Wilms tumor 1 (WT-1)-positive cells and thrombosis scores were estimated on *days −1* and *12*.

Staining and Morphological Analysis

Kidneys were fixed in 4% paraformaldehyde and embedded in paraffin. Parts of the kidney samples were incubated in graded (10–20%) sucrose-PBS solution and frozen for immunofluorescence or were fixed with 2% glutaraldehyde for transmission electron microscopy. Paraffin sections (2 μm) were processed for periodic acid-Schiff staining, periodic acid-silver methenamine staining, and immunostaining with specific primary antibodies, as shown in Table 1. Immunohistochemical staining was performed using standard procedures with an Avidin/Biotin Blocking Kit (Vector Laboratories, Burlingame, CA) and peroxidase-conjugated EnVision+Single Reagent (Dako, Glostrup, Denmark), and sections were visualized using diaminobenzidine (DAB substrate-chromogen system, Dako) or nitroblue tetrazolium (Roche Diagnostics, Mannheim, Germany) according to the manufacturers' instructions.

For immunofluorescence analysis, frozen sections and paraffin sections were used. Primary antibodies (β_1-integrin, synaptopodin, PAI-1, and CD31) were reacted with secondary antibodies labeled with Alexa 488 or 568 (Life Technologies, Carlsbad, CA) or rhodamine-conjugated secondary antibodies, respectively. Double immu-

Table 1. *Primary antibodies for immunostaining*

First Antibody	Application	Host Species	Dilution	Supplier
WT-1	IHC	Goat polyclonal antibody	1:200	Santa Cruz Biotechnology
PAI-1	IHC and IF	Rabbit polyclonal antibody	1:50 and 1:50	Santa Cruz Biotechnology
Synaptopodin	IF and IHC	Mouse monoclonal antibody	1:1 and 1:1	PROGEN Biotechnik
Fibrinogen	IHC	Rabbit polyclonal antibody	1:500	Dako Cytomation
uPAR	IE and IHC	Rat polyclonal antibody	1:30 and 1:50	R&D Systems
β1-Integrin	IF, WB, and IE	Rabbit polyclonal antibody	1:500 and 1:30	Novus Biologicals
α-Tublin	WB	Mouse monoclonal antibody	1:500	Sigma-Aldrich
CD31	IF	Rat polyclonal antibody	1:50	BD Pharmingen

IHC, immunohistochemistry; IF, immunofluorescence; IE, immunoelectronmicroscopy; WB, Western blot analysis.

nofluorescence was performed using standard procedures. Nuclear staining was performed using 4′,6-diamidino-2-phenylindole. For the quantitative determination of podocyte numbers, the WT-1-positive cells were counted in all glomeruli of each section on *days −1* and *8* (>30 glomeruli/mice), and at least 70 randomly selected glomeruli were counted on *day 12* under high-power magnification (×400). Average podocyte numbers per glomerulus were calculated on the basis of individual values. Thrombi and sclerosis were evaluated in periodic acid-silver methenamine-stained paraffin sections. Glomerular sclerosis and thrombosis scores were determined as follows. Each glomerulus was graded on a scale of *0–4*, representing the thrombotic or sclerotic area involving 0%, 1–25%, 26–50%, 51–75%, or >75% of the glomerulus, respectively. Glomeruli ($n > 70$) for each section were averaged and defined as the thrombosis score or sclerosis score per mouse, separately ($n = 6$).

RNA Extraction and Quantitative Real-Time PCR

Glomerular isolation was performed using ion powder perfusion and a magnet, as previously described (38). Total RNA was isolated using ISOGEN (Wako Pure Chemical Industries, Osaka, Japan). Total RNA was reverse transcribed using the Thermoscript RT-PCR System (Invitrogen, Karlsruhe, Germany) for first-strand cDNA. For quantitative analysis, all measured values were normalized to GAPDH gene expression using the $\Delta\Delta C_t$ method (C_t is threshold cycle), and results are presented as relative expression in arbitrary units. All primers used are shown in Table 2.

Western Blot Analysis

Samples were solubilized in RIPA buffer with protease inhibitors. Cytoplasmic proteins from cultured podocytes were extracted using a subcellular protein fractionation kit for cultured cells (Thermo Scientific, Pittsburgh, PA). Proteins were separated by 4–12% polyacrylamide gel electrophoresis (SDS-PAGE) and transferred to polyvinylidene difluoride membranes (PALL, Port Washington, NY). Blots were incubated with the primary antibodies shown in Table 1. After being washed in blocking solution, primary antibodies were detected using horseradish peroxidase-conjugated antibody (GE Healthcare, Buckinghamshire, UK) and a chemiluminescent substrate.

Table 2. *Sequence-specific primers for real-time PCR*

Gene	Sequence
Plasminogen activator inhibitor type 1	
Forward	5′-AGGATCGAGGTAAACGAGAGC-3′
Reverse	5′-GCGGGCTGAGATGACAAA-3′
Transforming growth factor-β	
Forward	5′-TGGAGCCTGGACACACAGTA-3′
Reverse	5′-TGTGTTGGTTGTAGAGGGCA-3′
Endothelial nitric oxide synthase	
Forward	5′-CCAGTGCCCTGCTTCATC-3′
Reverse	5′-GCAGGGCAAGTTAGGATCAG-3′
VEGF	
Forward	5′-CCAGCGAAGCTACTGCCGTCCA-3′
Reverse	5′-ACAGCGCATCAGCGGCACAC-3′
Desmin	
Forward	5′-GCGTGACAACCTGATAGACG-3′
Reverse	5′-GTTGGATTTCCTCCTGTAGTTTG-3′
Vimentin	
Forward	5′-GATCGATGTGGACGTTTCCAA-3′
Reverse	5′-ATACTGCTGGCGCACATCAC-3′

Cell Experiments

The immortalized mouse podocyte cell line (*passages 10–16*) used was a generous gift from Dr. Sakairi (Gunma University) (33). Cell differentiation was induced as previously described (39). All cell experiments were done under the following conditions and compared. Podocytes were treated in vitro with either uPA, PAI-1 alone, the PAI-1/uPA complex (PAI-1/uPA), or the PAI-1/uPA complex followed by anti-uPAR antibody (4 g/ml, R&D Systems, Minneapolis, MN) pretreatment (anti-uPAR + PAI-1/uPA). All compounds used were set by equimolar concentrations (5 nM). Glycosylated mouse PAI-1 (stable mutant) and active two-chain high-molecular-weight mouse uPA were purchased from Molecular Innovations (Novi, MI). The PAI-1/uPA complex was prepared by reacting 5 nM uPA with PAI-1 for 10 min at 37°C (40). After acid treatment for tight cell adhesion (5, 6), podocytes in individual wells were treated with uPA, PAI-1, the PAI-1/uPA complex, or anti-uPAR antibody before PAI-1/uPA complex administration. Anti-uPAR antibody was prepared by preincubation for 30 min at 37°C before the addition of the PAI-1/uPA complex.

Podocyte Detachment Assay

The podocyte detachment assay was analyzed by two blinded observers (M. Nagata and T. Ueno). Equal numbers of podocytes (4×10^3 cells/well) were seeded on 24-well plates precoated with collagen type I (0.03%) and treated under each condition described above.

Biotinylation of Cell Surface Protein Experiments

Surface biotinylation was performed using the Cell Surface Protein Isolation Kit (Pierce, Rockford, IL). Differentiated podocytes were biotinylated for 30 min at 4°C with 0.25 mg/ml sulfo-NHS-SS-biotin and then sonicated with lysis buffer. The biotinylated protein was extracted by an incubation with streptavidin-coupled beads for 60 min. After this, sample buffer containing DTT was added to the extraction buffer, and samples were incubated for 60 min using an end-over-end mixer followed by centrifugation. This procedure was performed for podocytes treated with uPA, PAI-1, the PAI-1/uPAR complex, or anti-uPAR + PAI-1/uPAR, and β_1-integrin expression was estimated by Western blot analysis.

Extraction of the Cytosolic Fraction

We used a subcellular protein fractionation kit for cultured cells (Thermo Scientific). Cells were detached by trypsin EDTA acid and

then centrifuged at 500 *g* for 5 min. After cells were washed, they were transferred to a microtube and pelleted by centrifugation at 500 *g* for 3 min. The cell pellet was obtained by discarding the supernatant. After this, cell extraction buffer with protease inhibitors was added and incubated with gentle mixing for 60 min at 4°C. The supernatant was immediately extracted as the cytoplasmic fraction after centrifugation at 500 *g* for 5 min.

Immunofluorescence in Cultured Podocytes

Podocytes grown on collagen type I-coated coverslips were treated under each condition described above and fixed with 4% paraformaldehyde in PBS. After being blocked with 50 mM glycine-PBS, podocytes were incubated with anti-uPAR antibody or anti-β_1-integrin antibody overnight followed by secondary antibodies conjugated with Alexa 488 (Life Technologies) or rhodamine for 2 h.

Double Immunogold Labeling of Ultrathin Cryosections

uPA- and PAI-1/uPA complex-treated cells were fixed in periodate lysine paraformaldehyde fixative for 6 h, pelleted, and then resuspended in 2.0% agarose (Wako Pure Chemical Industries, Osaka, Japan) as previously described (23). The grids were incubated on anti-β_1-integrin antibody and anti-uPAR antibody in 1% BSA overnight at 4°C followed by secondary antibodies of goat anti-rabbit 5-nm gold (BB, Cardiff, UK) or goat anti-rat 10-nm gold (BB) for 2 h at room temperature. Sections were stained with both uranyl acetate and lead citrate and inspected under a transmission electron microscope (model JEM-1400, JEOL, Tokyo, Japan) at 80 kV.

Statistics

Results are presented as means ± SE. Comparisons between two groups were performed using two-tailed Student's *t*-tests. Comparisons between three or more groups were performed using nonrepeated-measures ANOVA. *P* values of <0.05 were considered statistically significant. In the figures, *P* values are indicated as $*P < 0.05$, $**P < 0.01$, and $***P < 0.001$.

RESULTS

Podocyte Depletion Caused Local Thrombotic Microangiopathy

NEP25/LMB2 mice developed significant proteinuria on *days 8* and *12* compared with control mice, and this was parallel with the decrease of WT-1 positive podocyte numbers, which was further diminished in glomeruli with thrombi compared with those without (Fig. 1, *A–C*). Serial section with fibrin immunostaining showed the association of local intracapillary thrombi with overlaying podocyte damage (Fig. 1, *D* and *E*). This was confirmed by double immunolabeling showing that segments lacking WT-1-positive cells were associated with fibrin in the corresponding capillary (Fig. 1*F*). Electron microscopy demonstrated that intracapillary coagulation debris and mesangiolysis were associated with degeneration or detachment of overlaying podocytes (Fig. 1*G*). These findings indicate that podocyte loss causes local thrombotic microangiopathy in this model.

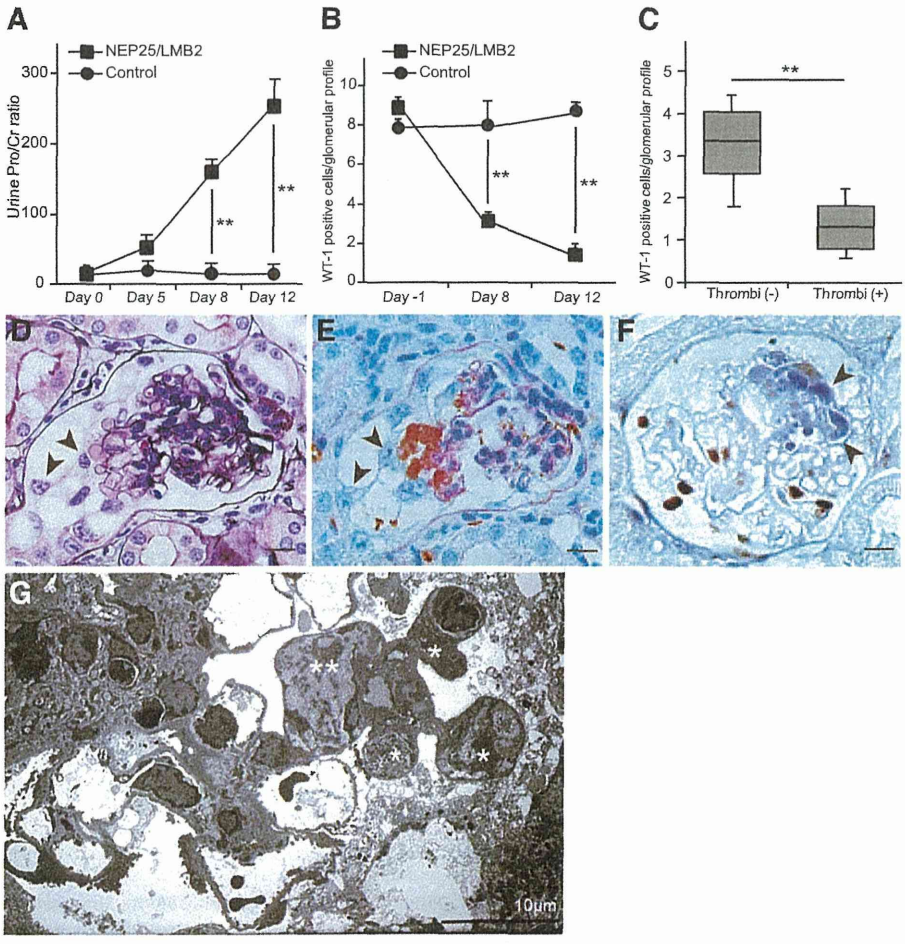

Fig. 1. Podocyte-specific injury evoked progressive proteinuria and microangiopathy. *A*: NEP25/LMB2 mice developed proteinuria on *day 5*, reaching significant levels on *days 8* and *12*, compared with control mice ($n = 6$ mice/group). Urinary Pro/Cr ratio, urinary protein-to-creatinine ratio. $**P < 0.01$. *B*: the number of Wilms tumor 1 (WT-1)-positive podocytes was significantly reduced in NEP25/LMB2 mice ($n = 6$) compared with control mice ($n = 6$). $**P < 0.01$. *C*: in NEP25/LMB2 mice, glomeruli without thrombi [Thrombi(−)] had significantly greater numbers of WT-1-positive cells compared with glomeruli with thrombi [Thrombi(+)] on *day 12*. Average numbers of glomeruli of glomeruli without and with thrombi were 27.1 ± 7.61 and 73.6 ± 11.4, respectively. $**P < 0.01$. *D*: representative glomerular features of NEP25/LMB2 mice on *day 12*. Thrombi were detected at the site of podocyte injury (arrowhead, periodic acid-silver methenamine). *E*: fibrinogen immunostaining on serial sections from *D* showing fibrinogen (brown) in the glomerular tuft with injured podocytes (arrowhead, counterstained with periodic acid-Schiff). *F*: double immunolabeling with fibrinogen (blue) and WT-1 (brown). Fibrinogen was found at the site where WT-1 disappeared (arrowhead). Original magnification: ×400. Scale bars = 15 μm in *D–F*. *G*: transmission electron microscopy (EM) of the glomerulus in NEP25/LMB2 mice on *day 12*. Intracapillary coagulation debris (*) and mesangiolysis (**) were associated with degeneration or detachment of overlaying podocytes. Original magnification: ×400. Scale bar = 10 μm.

Endothelial PAI-1 Upregulation as an Early Response to Podocyte Injury

In NEP25/LMB2 mice, glomerular mRNA of VEGF and endothelial nitric oxide synthase (eNOS) was decreased with the thrombosis score on *day 12* (Fig. 2, *A–C*). Transforming growth factor-β and PAI-1 transcripts were significantly elevated on *day 1* in NEP25/LMB2 mice after LMB2 injection (Fig. 2, *D* and *E*). In NEP25/LMB2 mice on *day 1*, PAI-1 was expressed in a diffuse and global pattern and colocalized with the endothelial cell marker CD31 by double immunofluorescence, whereas PAI-1 was not expressed in control mice (Fig. 2*F*). At the later stage, on *day 12*, PAI-1 was expressed in preserved capillaries and podocytes (Fig. 2*G*). uPAR

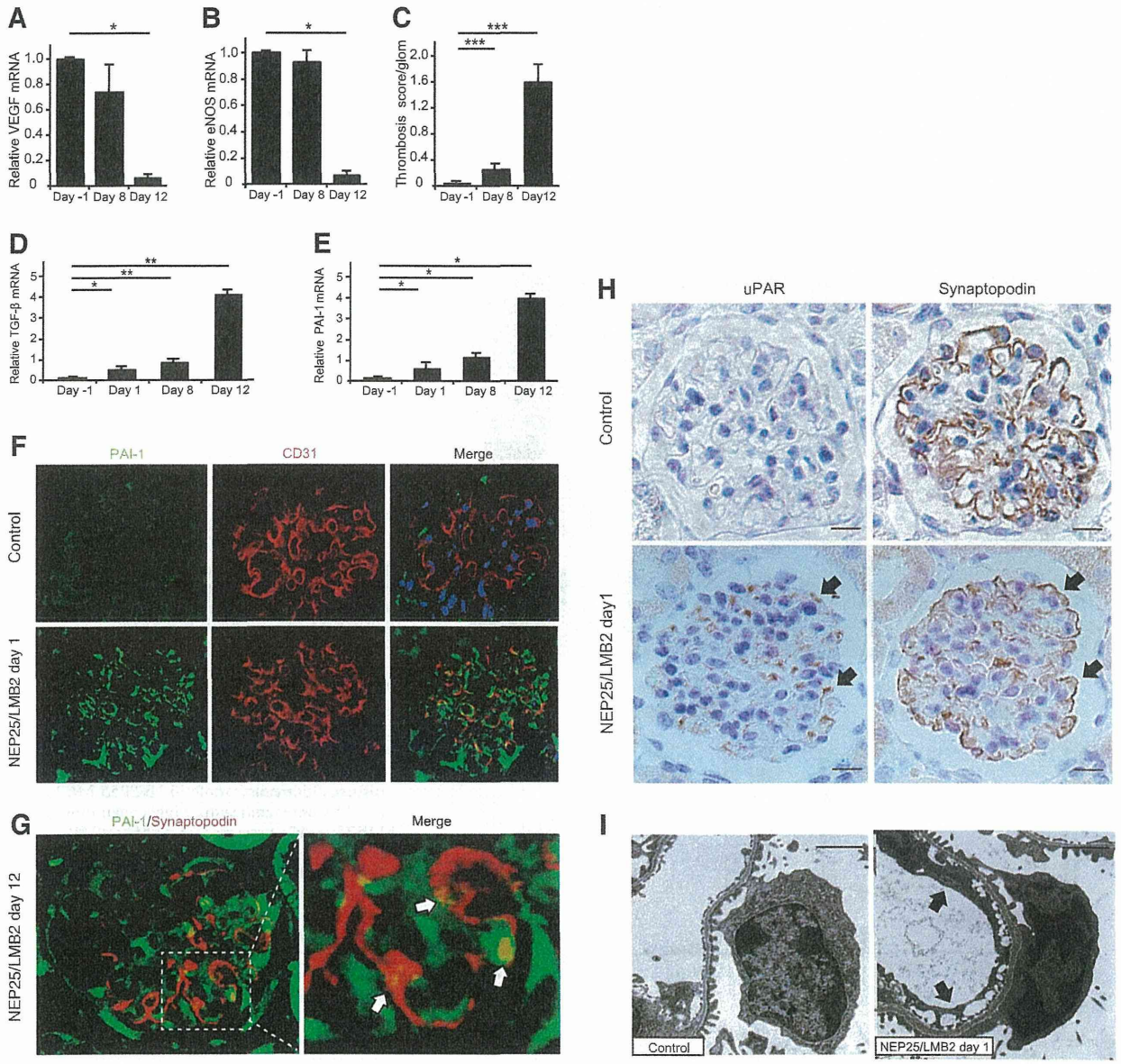

Fig. 2. Upregulation of plasminogen activator inhibitor type 1 (PAI-1) as an early endothelial response against podocyte injury. *A* and *B*: in NEP25/LMB2 mice, glomerular mRNA expression of the endothelial dysfunction markers VEGF and endothelial nitric oxide synthase (eNOS) was decreased on *day 12*. $*P < 0.05$. *C*: compared with *day −1*, the thrombosis score was significantly elevated on *day 12* in NEP25/LMB2 mice ($n = 6$). $***P < 0.001$. *D* and *E*: transforming growth factor (TGF)-β mRNA expression in isolated glomeruli (*D*) and relative PAI-1 mRNA (*E*). TGF-β mRNA was increased in NEP25/LMB2 mice on *day 1* and further increased on *days 8* and *12*. PAI-1 mRNA expression in isolated glomeruli was increased on *day 1* and further increased on *days 8* and *12*. $n = 5$ mice/group for each time point. $*P < 0.05$; $**P < 0.01$. *F*: double immunofluorescence of PAI-1 and CD31 expression in control and NEP25/LMB2 mice in glomeruli on *day 1*. Magnification: ×600. PAI-1 was absent in control mice, whereas it was expressed and colocalized with CD31 in NEP25/LMB2 mice. *G*: on *day 12*, PAI-1 was aberrantly expressed in the podocyte cytoplasm in NEP25/LMB2 mice. *H*: expression of urokinase plasminogen activator (uPA) receptor (uPAR) in NEP25/LMB2 mice on *day 1* as revealed by serial sections. uPAR was not expressed in control mice (*top*), whereas it was expressed mainly in podocytes in NEP25/LMB2 mice (*bottom*), as confirmed in synaptopodin staining by serial sections (arrows). *I*: electron microscopy showed endothelial cell swelling and loss of fenestra (arrows) accompanied with overlaying podocyte foot process effacement in NEP25/LMB2 mice compared with control mice on *day 1*. Scale bars = 2 μm.